The Journal of Chemical Physics

Absorption spectroscopy of heavy alkaline earth metals Ba and Sr in rare gas matrices—CCSD(T) calculations and atomic site occupancies

Cite as: J. Chem. Phys. **144**, 044308 (2016); https://doi.org/10.1063/1.4940688
Submitted: 02 November 2015 . Accepted: 08 January 2016 . Published Online: 29 January 2016

Barry M. Davis, and John G. McCaffrey

Absorption spectroscopy of heavy alkaline earth metals Ba and Sr in rare gas matrices—CCSD(T) calculations and atomic site occupancies

Barry M. Davis and John G. McCaffrey[a)]
Department of Chemistry, Maynooth University, National University of Ireland—Maynooth, County Kildare, Ireland

(Received 2 November 2015; accepted 8 January 2016; published online 29 January 2016)

Isolation of the heavier alkaline earth metals Ba and Sr in the solid rare gases (RGs) Ar, Kr, and Xe is analysed with absorption spectroscopy and interpreted partly with the assistance of *ab initio* calculations of the diatomic M·RG ground state interaction potentials. The $y^1P \leftarrow a^1S$ resonance transitions in the visible spectral region are used to compare the isolation conditions of these two metal atom systems and calcium. Complex absorption bands were recorded in all three metal atom systems even after extensive sample annealing. Coupled cluster calculations conducted on the ground states of the nine M·RG diatomics (M = Ca, Sr, and Ba; RG = Ar, Kr, and Xe) at the coupled cluster single, double, and non-iterative triple level of theory revealed long bond lengths (>5 Å) and shallow bound regions (<130 cm^{-1}). All of the M·RG diatomics have bond lengths considerably longer than those of the rare gas dimers, with the consequence that isolation of these metal atoms in a single substitutional site of the solid rare gas is unlikely, with the possible exception of Ca/Xe. The luminescence of metal dimer bands has been recorded for Ba and Sr revealing very different behaviours. Resonance fluorescence with a lifetime of 15 ns is observed for the lowest energy transition of Sr_2 while this transition is quenched in Ba_2. This behaviour is consistent with the absence of vibrational structure on the dimer absorption band in Ba_2 indicating lifetime broadening arising from efficient relaxation to low-lying molecular states. More extensive 2D excitation-emission data recorded for the complex site structures present on the absorption bands of the atomic Ba and Sr systems will be presented in future publications. © *2016 AIP Publishing LLC.* [http://dx.doi.org/10.1063/1.4940688]

I. INTRODUCTION

The literature on the spectroscopy of matrix-isolated barium is quite limited—a surprising situation considering the direct connection between rare gas (RG) matrix work and studies probing the behaviour of atomic barium in a variety of environments including He-nanodroplets,[1,2] solid and liquid helium,[3] and isolated on large rare gas clusters.[4–6] A wealth of data has been accumulated from these related systems yielding insights, for example, into the excited P states forming bubbles in liquid helium or size exclusion effects forcing surface attachment on Ar clusters. Further compounding the lack of published work, the limited literature that does exist on matrix-isolated atomic barium is in error in several regards. Thus, the original article published by Balling and Wright[7] (B&W) as a comprehensive study of the absorption and emission spectra Ba isolated in the three rare gas hosts Ar, Kr, and Xe is, in fact, restricted to results obtained in Ar. It turns out that the Ba/Kr spectra presented by B&W[7] are, as revealed in the present study, actually annealed Ba/Ar data and yet this article states that no effects were observed in "warm-up" experiments. The same authors also reported that emission was not observed in the Ba/Xe system, speculating that the formation of a Ba–Xe chemical bond precluded the isolation of atomic barium in solid xenon. The recent study by nEXOCollaboration,[8] done as part of the nEXP project [PRL **109**, 032505 (2012)] to determine the fundamental characteristics (mass) of neutrinos, demonstrated that emission does in fact occur in the Ba/Xe system. However, the attribution of certain bands as transitions of Ba ions indicated the existence of additional impurity species in the spectra of Ba/RG matrices. To address these basic deficiencies and resolve the substantial complexities in the Ba/RG systems, a systematic study of the optical spectroscopy of matrix-isolated barium has been undertaken in the three hosts Ar, Kr, and Xe.

An informative matrix absorption study was conducted by Miller *et al.*[9] on the closely related Mg, Ca, and Sr atoms isolated in the solid rare gases (sRGs) Ne, Ar, and Kr. This study also involved a magnetic circular dichroism (MCD) analysis. However, the spectra recorded for these lighter alkaline earth atoms were difficult to interpret due to complex band profiles. In an attempt to definitively characterise the spectroscopy of matrix-isolated barium, we have broadened the scope of this work to be a general study of M/RG samples which also includes the lighter alkaline earth metals Sr and Ca. Since Ca, Sr, and Ba all have $(ns)^2$ ground state electronic configurations, with n = 4, 5, and 6, respectively, similar van der Waals interactions with the host environment of the sRGs would be expected for all these atoms. These weak interactions have been calculated in this study with coupled-cluster methods. However, with increasing principal quantum numbers n, the site occupancies may differ due to the expanding sizes of the heavier metal atoms. Moreover, since the strongest electronic transitions of these atoms occur,

a)Email: john.mccaffrey@nuim.ie

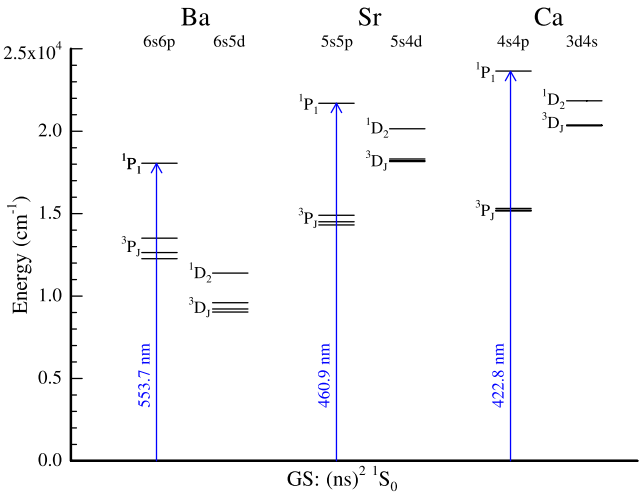

FIG. 1. An energy level diagram showing the excited states of the alkaline earth metal atoms Ba, Sr, and Ca which exist below 25 000 cm^{-1}. The resonance transitions of all three metal atoms occur in the visible/near-UV spectral regions at the specified wavelengths. Sr and Ca share many similarities, especially in having the D levels close to the resonance $^1P_1$ level. In contrast, the D states are lower than the ^3P in Ba such that the $^3D_1$ state the metastable level. For the two other metal atoms, it is the $^3P_0$ level.

as shown in Fig. 1, roughly in the same energy region, similar features should be present in the recorded spectra. With a goal to interpret these complex, multiple-site absorption bands, we have pursued a combined analysis of the matrix spectra for the three heavier $(ns)^2$ metal (M) atoms Ca, Sr, and Ba in the visible region. This global approach has proven successful in a previous M/Ne study from our group,[10] where the sites occupied by atomic Mg, Zn, and Cd were analysed in solid neon.

In the present contribution, we have undertaken a combined experimental and theoretical study to achieve tentative assignments of the sites occupied by Ca, Sr, and Ba atoms in Ar, Kr, and Xe matrices. This involved detailed comparisons of the features common to the absorption spectra recorded in the metal atom matrix systems while using accurate ground state interaction potentials for the M·RG (RG = Ar, Kr, and Xe) diatomics to evaluate possible site occupancies. The composition of the Ba/RG samples deposited was examined with two metal vaporisation methods—namely, electron bombardment and thermal vaporisation. This analysis was done primarily to examine for the presence of Ba ions or other metal impurities and to optimise the isolation of metal atoms versus small clusters. The region of the atomic resonance shows the presence of bands due to metal dimer absorptions showing the need for a careful and systematic study of sample preparation conditions. Details of the dimer photophysics are included in the present article. Those of atoms isolated in annealed matrix samples will be presented in a luminescence study nearing completion.

II. METHODS

A. Experimental

The vacuum apparatus and gas handling system used in this work have been described in previous publications by our group.[11,12] Typically, the pressure in the sample chamber was 1×10^{-7} mbar at room temperature, dropping to less than $\sim 5 \times 10^{-8}$ mbar when the sample window was cooled to 10 K. Metal vapour was generated in two different ways. The first was with electron bombardment of Ba or Sr pieces (Ba: Sigma Aldrich, 403334-10G, 99% purity, Sr: Sigma Aldrich, 343730-10G, 99% purity) held in a Mo crucible, as used in most of our previous metal atom work.[2] The second method involved resistive heating of a barium dispenser (Alvatec, Alvasource AE-3-Ba-50C). Thermal vaporisation was used in an attempt to preclude charged species, such as barium cations being deposited in our samples. The dispenser was mounted on a high vacuum electrical feedthrough which was attached to the front face of the sample chamber with a CF flange. A cylindrical stainless steel radiation shield and cap (attached to the base of the feedthrough) surrounded the dispenser. An aperture (5 mm in diameter) in the centre of the cap allowed the barium vapour to escape in the direction of the sample window with minimal radiative heating. The unit was positioned such that the centre of the dispenser was aligned with the centre of the CaF_2 window.

Once mounted under high vacuum, the dispenser was heated with a variac controlled electrical supply. Initial heating involved applying a low current (2-3 A) to melt the indium seal on the top of the dispenser. Ar gas, used as an inert environment in the dispenser compartment, was thereby released exposing the barium metal to vacuum. Higher currents (~6 A) were used for outgassing and ultimately to sublimate barium and produce a metal beam. The metal vapour was then co-condensed with the rare gases (Ar: BOC Gases, Research Grade C, Kr: Air Liquide, 99.998%, Xe: CK Special Gases, 99.999%) of choice onto the CaF_2 window. Samples were deposited at gas flow rates of 3 mmol/h for periods of 25-30 min. The temperature of the sample was monitored with a Scientific Instruments 9600-1 silicon diode which was secured to the copper holder of the sample window. The metal concentration, and hence composition of each matrix sample, was also varied. With electron bombardment, this was done by adjusting the filament current, using the metal flux monitor on the Omicron (model EFM3 UHV) evaporator as an accurate guide. Using the dispenser, this was achieved by varying the current supplied to the resistive heater.

The spectroscopic setup used for recording absorption spectra has been described in detail elsewhere.[11,12] Absorption scans were obtained either with a deuterium lamp (UV, 180–400 nm range) or a tungsten lamp (UV–Vis, 300–900 nm range) as light source and using a 0.3 m focal length Acton Research Corporation (ARC) model SpectraPro-300i monochromator, containing a 1200 grooves/mm diffraction grating blazed at 300 nm, for wavelength selection. Transmittance was recorded directly through the matrix sample and monitored using a Hamamatsu R928 PMT detector. Emission spectra were recorded perpendicular to the excitation beam with an ARC 0.5 m SpectraPro-500i monochromator fitted with three gratings, a 1200 g/mm and a 150 g/mm, both blazed at 300 nm and a 600 g/mm grating blazed at 500 nm. Two separate detectors were mounted on the SP-500i: (1) a Hamamatsu R928-P PMT operating in photon counting mode and maintained at −20 °C in a

Products for Research (Photocool, S600) cooled housing and (2) an intensified, time-gated charge coupled device (iCCD) detector Andor Technologies (iStar DH720) held at −15 °C by an integrated Peltier cooling system. A swing mirror in the SP-500i allowed the emitted radiation to reach the detector of choice. A Q-switched Nd:YAG (Quantel, YG980)/dye (Quantel, TDL90) laser combination was used with the nanosecond iCCD camera to record excited state lifetimes and high resolution excitation scans. The dyes Coumarin 460 Coumarin 540A, Rhodamine 6G, and LDS698 were used in this work.

B. Theoretical

Ground state potential energy curves (PECs) were calculated for the Ba·RG, Sr·RG, and Ca·RG (RG = Ar, Kr, and Xe) diatomics at the coupled cluster level of theory involving single, double, and non-iterative triple (CCSD(T)) excitation with a restricted Hartree-Fock reference wavefunction. These computations were implemented using the NWChem-6.5 (revision 26243-4) quantum chemistry package[13] running on a PC workstation (AMD64 quad-core 2.8 GHz processor) with the Linux Mint-17.1 (Cinnamon) operating system. The standard correlation consistent aug-cc-pVQZ basis set was employed for Ar and Kr atoms. The heaviest rare gas, Xe, was represented by the aug-cc-pVQZ-PP basis set with a small core, fully relativistic ECP28MDF effective core potential (ECP).[14,15] For atomic Ca, Sr, and Ba, the aug-cc-pVQZ-PP basis set[16,17] was used in conjunction with the respective relativistic ECP10MDF, ECP28MDF, and ECP46MDF effective core potentials.[18] All the electrons of Ar and Kr were correlated, as were all of the non-ECP electrons of Xe, Ca, Sr, and Ba. Boys and Bernardi[19,20] counterpoise correction was computed at each point to account for basis set superposition error (BSSE). The potential energy curves were generated by cubic spline interpolation of the single point energy values. Binding energies were determined by taking the energy difference between the minima with the values existing at 50 Å, taken to be the asymptotic limit. The single point energy values were computed in steps of 0.1 Å in the range from 3.5 to 6 Å. This was done in order to accurately describe the repulsive wall and minimum of the potential energy curves. As the long range portion of the curve changes more gradually, steps of 0.2 Å and 0.5 Å were adopted and sufficiently accurate in the ranges from 6 to 8 Å and 8 to 10 Å, respectively.

III. RESULTS AND ANALYSIS

A. Initial Ba/RG samples

The first matrix absorption spectra recorded for samples prepared by co-depositing barium vapour with Ar and Xe at 10 K are shown by the black traces in Fig. 2 in the range 400–650 nm. In addition to the strong Ba 6s6p $^1P_1 \leftarrow (6s)^2$ $^1S_0$ resonance transition at approximately 550 nm in Xe, a number of bands are also located at 460 nm. Because of their spectral positions, these bands were thought initially to be small amounts of Ba ions isolated on deposition. The

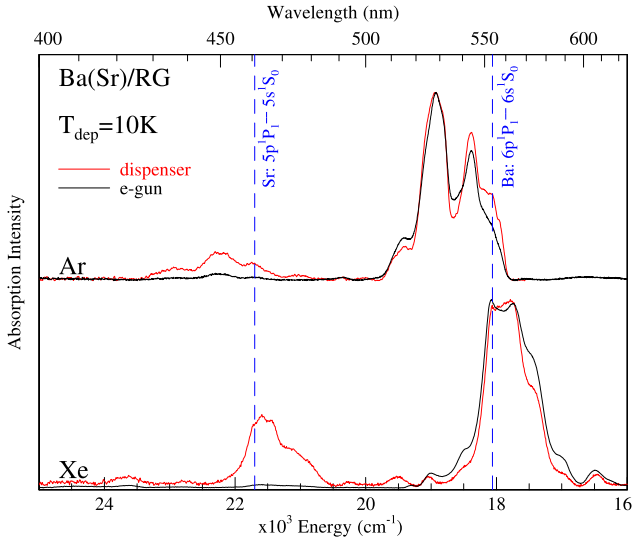

FIG. 2. Absorption spectra recorded for Ba/Ar and Ba/Xe samples at 10 K in the visible spectral region. The solid black traces were recorded for samples formed with electron-bombardment and the red traces show the result of using the thermal dispenser. As revealed by the indicated transitions, significant amounts of atomic Sr are present in both matrices. The comparison further reveals the greater extent of Sr contamination in the samples formed from thermal deposits.

suspicion was that the atomic cation was being generated in the e-bombardment source used for Ba metal vaporisation and to investigate this possibility, the dispenser (getter) source described in Sec. II (Alvatec, Alvasource AE-3-Ba-50C) was used instead. The results of changing to the thermal source are presented as the red traces in Fig. 2. A cursory inspection reveals that the dispenser spectra actually contain much more barium "ions" than was observed with the electron bombardment (e-gun) source. Because of this nonsensical finding, obtained with a low energy thermal source, checks were made of the barium metal being used—only to make a rather surprising discovery.

It turns out that strontium is a small (~0.8%) but persistent impurity in barium metal.[21] Having a similar melting point (1040 K) to barium but with a much lower boiling point (1650 vs. 2171 K), strontium vaporises much more readily. The large boiling point difference exaggerates, as evidenced by the Xe scans shown in Fig. 2, the extent of Sr contamination in "Ba" samples formed as thermal deposits far above its impurity level. Knowing that Sr was present in the barium metal we were using, a systematic study of the vaporisation conditions was conducted to minimise the amount of Sr deposited in the Ba/RG matrix samples. Our study revealed that the presence of the Sr impurity is considerably smaller with the bombardment source. In contrast to the dispenser source, which melts the entire bulk volume of the barium, the electron-beam only melts a spot on the surface of the metal. Thus, samples deposited with the e-gun contain, as shown in Fig. 2, much less Sr, suggesting that the Sr contamination can be depleted in the local area (spot) of the bulk barium metal heated by the e-beam. This depletion could be completed prior to deposition, during the 15 min warm-up time required to stabilise the metal flux. Provided the metal flux was kept low during the deposition (with a small e-beam current),

Ba/RG samples largely free of Sr could be formed with e-bombardment. The presence of Sr impurity has previously been observed for Ba isolated in liquid helium and solid He matrices.[3] It should be pointed out that some of the novel species identified in the excitation/emission spectra of Xe samples formed from the co-deposition of Ba^+ beam in the recent study done in matrices[8] are in fact atomic strontium. In order to properly characterise the spectroscopy of the Ba/RG samples, we have also investigated the spectroscopy of matrix-isolated Sr. Accordingly, the absorption spectra recorded of pure Sr/RG samples are presented in Section III E. The results obtained for the "purest" Ba/RG samples, formed following the procedure previously outlined, will now be presented.

B. Ba/RG concentration studies

A concentration study made for the isolation of barium in argon is presented in Fig. 3. Traces (a)–(c) were recorded for samples deposited at 19 K with high, medium, and low metal fluxes, respectively. Trace (d) presents a 9.8 K/low flux deposition which contains predominantly isolated Ba atoms. The spectra presented in Fig. 3 reveal a number of important trends regarding the isolation conditions of the metal. First, there is a steady intensity increase for the absorption features labelled I–III, centred at 747.4, 568.5, and 491.5 nm, respectively, with respect to the atomic features present in the 10 K spectrum (trace (d)) upon increasing the metal flux. Second, the nature of the bands in the vicinity of the resonance atomic 6s6p $^1P_1 \leftarrow (6s)^2\ ^1S_0$ transition at approximately 554 nm get progressively more complex and broader with increasing concentration. Third and in stark contrast to the 550 nm region, the pair of absorption bands present in the near-UV region (at approximately 320 nm) change very little with increasing metal loading from the high dilution, low temperature sample shown in trace (d). Each of these three characteristics will be analysed in turn.

Normalising each spectrum to band III at 491.5 nm reveals that a constant intensity ratio of bands I-III is maintained throughout the concentration study. Combining this behaviour with the growth patterns described above indicates that these absorptions belong to the same species. As all three bands are present, albeit extremely weakly, in the low temperature deposition (the most atomic) sample (d), a tentative assignment to barium dimer (Ba_2) is made. Support for this assignment comes from a resonant, two-photon ionization (R2PI) study of Ba_2.[22] With the R2PI technique, an excitation spectrum of mass-resolved Ba_2 was obtained which consisted of a group of 12 vibrational bands in the 740–764 nm region. This series was assigned to the $(2)^1\Sigma_u^+ - X(1)^1\Sigma_g^+$ transition of barium dimer. Although unstructured in the present Ar matrix spectra, the broad feature (band I) at 747.4 nm is thereby attributed to this molecular transition. Based on the same behaviour observed in the concentration study, the other two features (bands II and III) are also assigned to Ba_2.

Absorption spectra of the three Ba/RG systems (RG = Ar, Kr, and Xe), deposited at high temperature with a medium-low metal flux, are presented together as the solid grey traces in Fig. 4. Concentration and temperature studies conducted on the heavier RG systems yielded results analogous to that outlined for Ba/Ar. Thus, three sets of absorption bands "grow in" in unison. The highest energy feature in Kr (Xe) is located at 508.8 (524.6) nm. Immediately to the red of the $^1P_1$ line, a series of bands are observed at 573.3, 583.1, and 590.6 (588.6, 606.2, and 614.3) nm. The lowest energy feature consists of a broad band centred at 760.6 (771.8) nm, blue-shifted in relation to the atomic $^3P_1$ transition shown in Fig. 4. As with Ba/Ar, these absorptions are assigned to barium dimer, with the lowest energy bands associated with the $(2)^1\Sigma_u^+ - X(1)^1\Sigma_g^+$ transition. Although the spectra shown in Fig. 4 were recorded with a resolution of 0.1 nm, vibrational fine structure was not observed on any of the barium dimer bands in three RG solids examined in the present study.

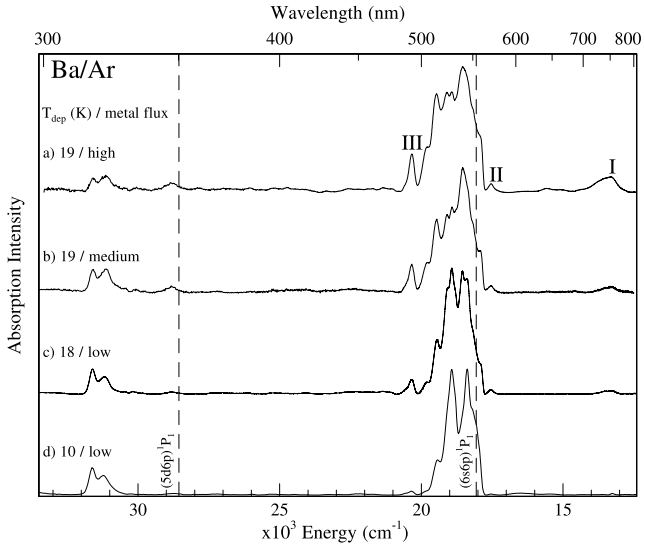

FIG. 3. A concentration study of the isolation of Ba in Ar samples at the specified deposition temperatures and metal fluxes. Two spectral regions of interest exist—one in the visible, the other in the near-UV. The most clearly defined metal dimer bands are indicated by the labels I–III.

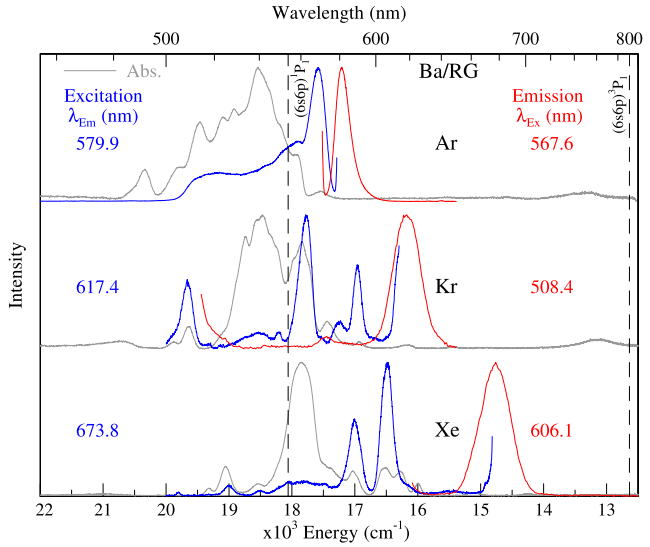

FIG. 4. A comparison of the barium dimer emission recorded in the three rare gases. The red and blue traces show the emission and excitation spectra, respectively, while the absorption spectra are shown in grey. Of particular note is the increasing Stokes shift in the xenon system.

C. Ba/RG barium dimer (Ba_2) emission

The Ba/Ar concentration study shown in Fig. 3 reveals that non-atomic absorption bands overlap the resonance 6s6p $^1P_1 \leftarrow (6s)^2\ ^1S_0$ atomic region with increasing metal loading. To extract these bands, excitation spectra were recorded for the relatively weak, red-shifted emission they produce in each host. The emission spectra, shown by the red traces in Fig. 4, have band maxima centred at 580.9, 617.4, and 676.8 nm in Ar, Kr, and Xe, respectively. The corresponding excitation spectra, recorded monitoring each of the aforementioned emission wavelengths, are represented by the solid blue traces. The excitation profiles recorded in Kr and Xe show a clear resemblance and allow for a definitive connection to be made with partly resolved features present in the absorption spectra (grey traces). For Kr (Xe), the absorption/excitation bands at 508.8 (524.6), 562.8 (588.6), 579.4, and 589.6 (606.2) nm share a common emission and are therefore associated with the same molecular species, Ba_2. The excitation spectrum of Ba_2 recorded in Ar appears simpler, consisting of one intense band centred at 568.5 nm and a broad wing extending up to 500 nm. The Ba_2/Kr results shown in Fig. 4 demonstrate the advantage of excitation spectroscopy over absorption alone. For instance, the band located at 562.8 nm was a barely evident shoulder on the intense atomic $^1P_1 \leftarrow {}^1S_0$ absorption but has been fully resolved and is clearly identified in the excitation scans.

The photophysical characteristics of the observed Ba_2 emission in the three rare gas hosts are collected in Table I. Lifetimes of 6 ns were recorded in Ar and Kr while the value in Xe is longer, in the region of 9 ns. Particularly pronounced in Table I, and evident in Fig. 4, is the variation in the Stokes shifts in the three rare gas solids studied—it increases by more than a factor of 4 from a value of 375 cm^{-1} in Ar to 1721 cm^{-1} in Xe, indication of a strong interaction between the metal dimer and the heaviest host. It is important to mention that the emission scans shown in Fig. 4 were made beyond 850 nm in all three RGs but no additional, lower energy dimer emission was observed in these low flux/high temperature samples. Furthermore, direct excitation of the dimer absorption band between 720 and 800 nm also did not yield any emission out to the limit of our detection, which is around 900 nm.

D. Ba/RG barium atom (Ba) features

Absorption spectra recorded for the three Ba/RG matrix systems are presented in Fig. 5 for samples formed at 10 K (black traces) and annealed (red traces) to the temperatures specified in the plot. Electron bombardment and low metal fluxes were employed during these depositions to reduce Sr contamination but also to minimise the formation of barium metal aggregates. The visible spectra, presented in the panel on the right hand side, consist of strong bands in the vicinity of the resonance (6s6p) $^1P_1 \leftarrow (6s)^2\ ^1S_0$ transition of atomic barium centred at 553.7 nm in the gas phase,[23] while the spectra in the near-UV region (left hand panel) appear quite different in the three hosts studied. The bands in this region are much weaker than in the visible—an indication of their relative absorption strengths can be gleaned from the Ba/Ar results shown in Fig. 3 where the entire spectral range is shown on a common intensity scale. While the weaker near-UV bands cannot immediately be associated with any of the indicated atomic gas phase transitions (shown by the vertical blue lines), the following analysis allows tentative assignments to be made.

1. Visible transitions

The dominant absorption feature in Ba/Ar is complex exhibiting a series of overlapping bands with peaks located at 514.2, 528.4, 543.9, and 554.0 nm. Shown also in Fig. 5 are the results of annealing to 30 K. From a comparison of the freshly deposited and annealed scans, it is evident that the features to the red are greatly reduced with annealing leaving at least three well resolved bands. Examination of the red trace in the top panel of Fig. 5 reveals that all three absorption bands are located to the blue of the gas phase $^1P_1 \leftarrow {}^1S_0$ transition, shown by a dashed vertical line. A matrix shift of +855 cm^{-1} exists on the central, most intense band at 528.7 nm. It should be pointed out that the annealed Ba/Ar spectrum shown in

TABLE I. A summary of the photophysical characteristics extracted for the emission of barium dimer (shown in Fig. 4) in the vicinity of the atomic resonance transition. The δ parameter indicates the shift of the dimer bands with respect to the atomic $^1P_1 - {}^1S_0$ transition, while SS is the Stokes shift between the emission and the lowest energy excitation band. From the values listed, the Stokes shift increases more than 4-fold from Ar to Xe indicating a strong interaction of the dimer and its hosts, especially in xenon.

Ba_2		Excitation			Emission				
RG	Band	λ (nm)	ν (cm^{-1})	δ (cm^{-1})	λ (nm)	ν (cm^{-1})	δ (cm^{-1})	SS (cm^{-1})	τ_{obs} (ns)
Ar	1	491.2	20 358	2298					
	2	541.8	18 457	396					
	3	568.5	17 590	−470	580.9	17 215	−846	375	6
Kr	1	508.4	19 669	1609					
	2	562.8	17 768	−292					
	3	579.4	17 259	−801					
	4	589.6	16 961	−1099	617.4	16 197	−1863	764	6.3
Xe	1	524.4	19 069	1009					
	2	588.6	16 989	−1070					
	3	606.2	16 496	−1564	676.8	14 775	−3285	1721	8.8

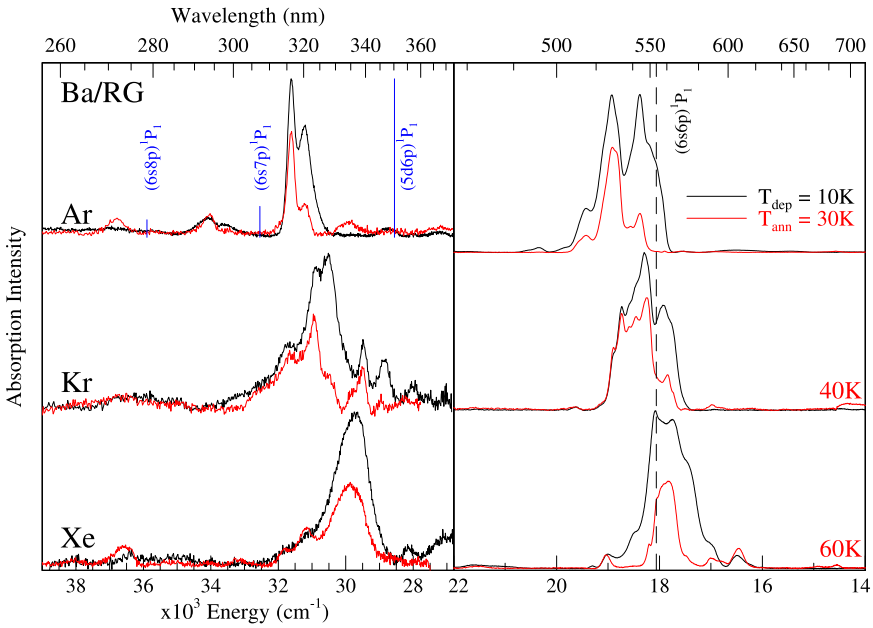

FIG. 5. A summary of the absorption spectra recorded at 10 K for the most dilute Ba/RG matrix samples in the visible and near-UV spectral regions. The black traces are the freshly deposited samples, while the red traces are those recorded after annealing to the specified temperatures in solid Ar, Kr, and Xe. The removal of the red sites is a feature common to all three matrix systems.

Fig. 5 is the same as the transmittance spectrum shown in Fig. 2 of B&W's publication and erroneously attributed in Ref. 7 to Ba/Kr. The transmittance spectrum shown in Fig. 1 of that publication matches the absorption shown by the black trace in Fig. 5 that was recorded on deposition of Ba/Ar. It pertains to a sample containing large amounts of the thermally unstable red site.

The results obtained for Ba/Ar are extended in Fig. 5 to include the two other rare gas matrices studied. For Ba/Kr, the dominant feature is centred at 537.8 nm while in Xe it is at 557.7 nm. A progressive red shift of the band centre is observed from Ar (+855 cm^{-1}), Kr (+536 cm^{-1}) to Xe (−130 cm^{-1})—an effect of the increasing rare gas polarizability. As in the Ba/Ar system, annealing removes the red features leaving a single dominant band in Ba/Xe and a complex profile in Ba/Kr. Despite this complexity, spectral assignment is straightforward based on dominance and location of these bands which accordingly are assigned as the solid state equivalent of the (6s6p) $^1P_1 \leftarrow (6s)^2\ ^1S_0$ transition of atomic barium. Due to the relatively weak van der Waals forces responsible for the barium-rare gas interaction (see the results of coupled-cluster calculations ahead), the energy of the solid-phase atomic transition is not expected to differ greatly from that of the free atom.

2. Near-UV transitions

The third key aspect identified in the initial Ba/Ar absorption spectra shown in Fig. 3 concerns the existence of previously unreported near-UV features consisting of a resolved doublet around 320 nm. A more detailed and extensive view of this spectral region is presented by the top trace in the left panel of Fig. 5 revealing the location of the intense doublet is at 316.2 and 320.3 nm. A weaker doublet exhibits peaks at 293.4 and 297.6 nm. Concentration studies conducted on the Ba/Ar system indicate, as shown in Fig. 3, that the intensities of both doublets track the resonance atomic 6s6p $^1P_1$ absorption under all metal/argon loadings—provided the latter is not fully absorbing. Accordingly, these bands are attributed to atomic barium. The two most intense gas phase[23] atomic lines occurring in this spectral region are the (5d6p) $^1P_1 \leftarrow {}^1S_0$ (6s^2) transition at 350.21 nm and the (6s7p) $^1P_1 \leftarrow {}^1S_0$ (6s^2) transition at 307.24 nm. Their relative intensities in the gas phase[23] are reported as 860 and 168, respectively, a ratio of approximately 5:1 as indicated by the vertical blue lines in Fig. 5.

The measured integrated areas of the two Ar matrix absorption profiles yield a ratio of approximately 6:1, in good agreement with the gas phase value. From the intensity correspondence evident in Fig. 5, it is clear that the absorption doublet centred at 318 nm arises from the (5d6p) $^1P_1 \leftarrow {}^1S_0$ (6s^2) transition of atomic barium while that centred at 295 nm is the solid state equivalent of the (6s7p) $^1P_1 \leftarrow {}^1S_0$ (6s^2) transition with a matrix shift of +1350 cm^{-1}. The location of the (6s8p) $^1P_1$ level is not obvious in the absorption spectra recorded for freshly deposited Ar samples. However, a band arises at approximately 270 nm after annealing (red trace) which is possibly due to this transition.

The absorption bands located at 326 nm in Kr and 336 nm in Xe are assigned to the atomic (5d6p) $^1P_1 \leftarrow {}^1S_0$ (6s^2) transition. In Ar, Kr, and Xe, the respective gas phase to matrix shift is calculated (from the band centre) as approximately 2892, 2121, and 1208 cm^{-1}. The large matrix blue-shift of approximately +2892 cm^{-1} present on the 318 nm band in argon is consistent with the fact it involves a two electron transition—the excited [Xe]5d6p electronic configuration is accessed from the [Xe]6s^2 ground state. From the signal-to-noise ratios evident in the three spectra shown, it would appear that the strength of the (5d6p) $^1P_1 \leftarrow {}^1S_0$ (6s^2) transition is reduced in Kr and Xe matrices compared to Ar. However, the integrated areas of the absorption profiles are very similar in all three rare gas solids. The weaker intensities are compensated by broader spectral widths in Kr and Xe. In contrast to the two atomic transitions discussed, analysis of the (6s7p) $^1P_1 \leftarrow {}^1S_0$ (6s^2) atomic transition, which was observed at approximately 295 nm for Ba/Ar, cannot be extended to all three RGs.

Weakly absorbing in Ar, this transition could not be identified in the absorption spectra of either Ba/Kr or Ba/Xe.

E. Sr/RG samples

Sr vapour, generated via electron bombardment of pure strontium metal, was co-condensed with high purity Ar, Kr, and Xe gas to form matrix-isolated Sr/RG samples. These data were initially used to identify Sr contamination in the first Ba/RG samples prepared. However, these absorption spectra will now be analysed to extract the behaviour of matrix-isolated strontium with regard to site occupancy of this lighter alkaline earth atom.

1. Concentration studies

As done with the matrix-isolated barium system, a concentration study was conducted on Sr/RG samples the results of which are presented for Sr/Ar in Fig. 6. The sample with the highest metal loading, shown in trace (a), presents the most complex spectrum but from a comparison with the most dilute sample (trace (d)), most of the non-atomic features can be attributed to dimer absorptions. The most prominent of these bands are indicated on trace (c) with the labels I-III. The lowest energy dimer feature, band I, is shown on an expanded scale on the right of the figure. In contrast to the equivalent Ba_2 band (shown in Fig. 3), this transition of Sr_2 shows resolved vibrational structure with an average splitting of 64 cm^{-1}.

2. Sr/RG strontium dimer (Sr_2) emission

Sr_2/RG emission and excitation spectra are shown in Fig. 7 while the extracted photophysical parameters are collected in Table II. A comparison with the equivalent Ba_2 plot shown in Fig. 4 reveals that the diatomics of these two elements exhibit very different emission. Sr_2 clearly shows resonance emission from the lowest energy transition (band I) at approximately 780 nm while Ba_2 produces none from this band. The lack of emission in the latter is most likely due to the density of molecular states which arise from the multitude of atomic barium D and P level asymptotes in this region. A comparison of the atomic energy levels of both elements is provided in Fig. 1, revealing the simplicity of the Sr (and Ca) and the complexity of Ba, due to the existence of the ^{1}D and ^{3}D states in the vicinity of the ^{3}P.

The Ar excitation scans shown in Fig. 7 establish that absorption band II, located at approximately 560 nm (see Fig. 6), is indeed a dimer band. Examination of the Kr and Xe excitation scans shown in Fig. 7 reveals that the atomic features are much more prominent in the dimer emission of the heavier rare gases. This is especially evident in the Sr/Xe scans shown in the bottom panel of Fig. 7 and arises because efficient $^1P \rightarrow {}^3P$ intersystem crossing (ISC) produces intense atomic Sr $^3P_1$ state emission in Xe, which coincides spectrally with the dimer emission. Details of the Sr atom emission in the sRGs will be presented elsewhere.[24] In any case, the resolved vibrational structure present on the 740 nm excitation band in Sr/Xe establishes that this is indeed a dimer transition.

A summary of the photophysical characteristics of the Sr_2 dimer band I in Ar is provided in Fig. 8 and the extracted data are collected in Table II. From a single exponential fit of the recorded emission decay curve, shown on a semi-log plot on the upper right in Fig. 8, a lifetime of 15.5 ns is obtained for the 780 nm band. The recorded decay curves were found to be independent of temperature up to 18 K, the highest value used, so 15.5 ns is accordingly identified as the radiative lifetime of the $^1\Sigma_u^+$ state of Sr_2 in Ar. With a lifetime of 15 ns, this clearly corresponds to a fully allowed molecular transition. The excitation scan shown by the blue trace in Fig. 8 was recorded by scanning the dye laser (with the LDS 698 dye) while recording the emission with the iCCD camera. The vibronic structure present on the excitation scan is better resolved than in the absorption scan (shown directly above) but attempts at conducting a

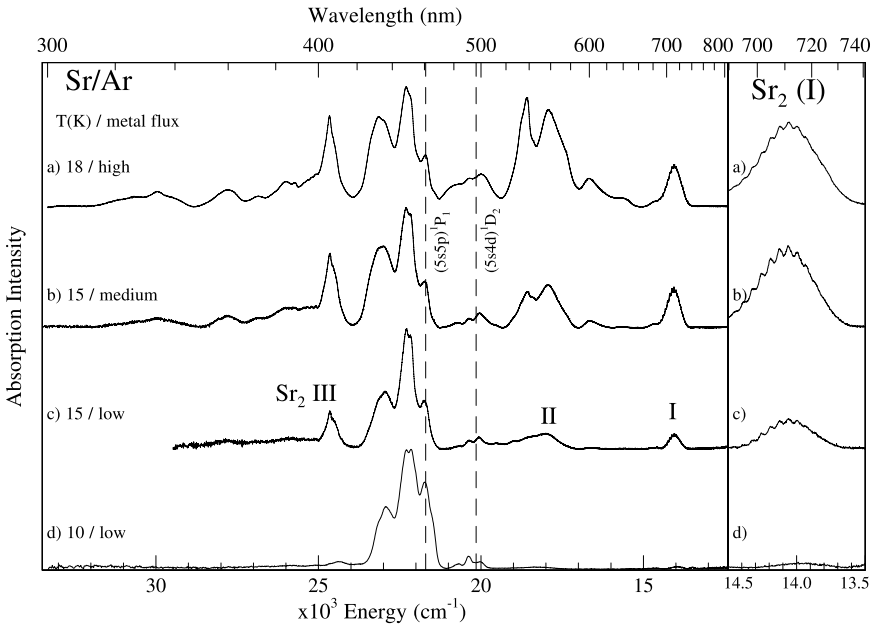

FIG. 6. A concentration study of the isolation of Sr in Ar samples at the specified deposition temperatures and metal fluxes. Only a single spectral region of interest exists here. The panel on the right shows resolved vibrational structure on the lowest energy Sr dimer band labelled I in the wide range plot.

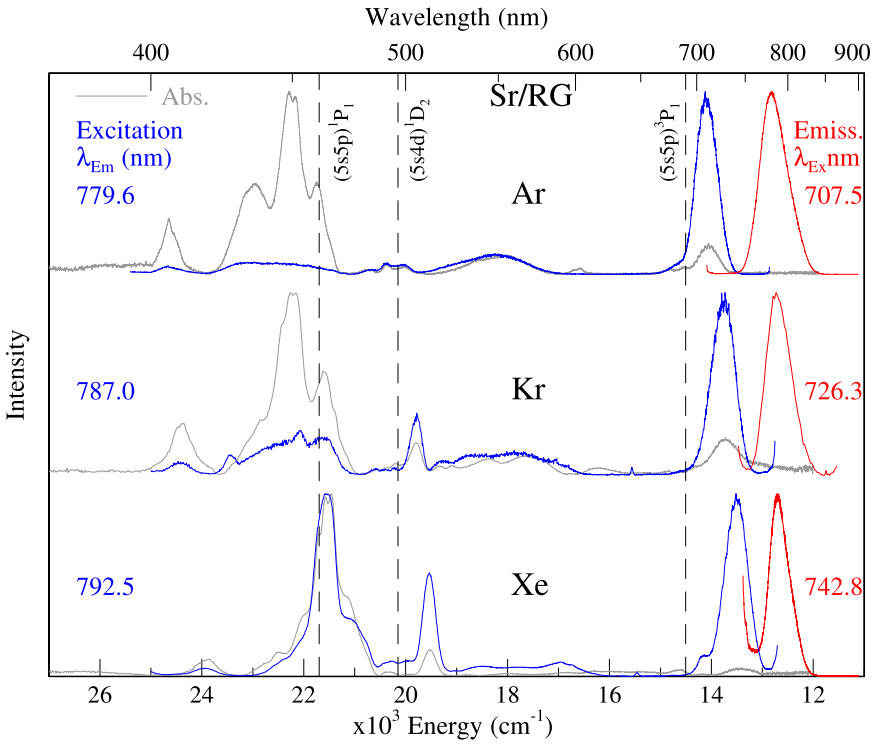

FIG. 7. A comparison of the strontium dimer emission recorded in the three rare gases. The red and blue traces show the emission and excitation spectra, respectively, while the absorption spectra are shown in grey. In contrast to the Ba_2 emission shown in Fig. 4, the Stokes shift on this transition is much less matrix dependent and appears least in the xenon system.

Birge-Sponer analysis of the resolved vibrational structure present in the laser induced fluorescence excitation spectra proved unsuccessful. The reason appears to be due to strongly overlapping bands arising from several isotopologues present in the spectrum. A mass resolved detection technique, such as R2PI, would address this issue. While there is no overlap between the excitation and emission profiles, the band origin of the molecular transition in Ar is tentatively attributed to the commencement of the emission at 13 500 cm^{-1}.

Comparison of the Sr_2 emission data in Table II with that provided in Table I reveals different behaviours to that observed for Ba_2. In particular, the Stokes shifts are small for Sr_2 emission and roughly the same in all three rare gas hosts. In contrast, those observed for Ba_2 are large and increase greatly in Xe.

3. Sr/RG strontium atom (Sr) features

The absorption spectra recorded following co-deposition of Sr vapour with the rare gases at 10 K, under conditions of low metal loading, are shown in Fig. 9. In contrast to the Ba/RG systems, the observed Sr features are present only in the visible spectral region from 400 to 520 nm. The dominant absorption bands are centred at 450.0, 457.4, and 467.7 nm in Ar, Kr, and Xe, respectively. These features are assigned to the resonance (5s5p) $^1P_1 \leftarrow {}^1S_0$ ($5s^2$) transition of atomic Sr, which occurs at 460.862 nm in the gas phase.[23] In addition to these bands, a series of weaker absorption peaks are clearly observed to the red of the $^1P_1$ line. In Ar (Kr, Xe), these peaks are located at 481.9 (484.1, 492.2), 491.0 (492.2, 501.7), and 499.3 (505.4, 511.6) nm. The spectra presented in Fig. 9 were recorded for highly atomic samples, with no evidence of the characteristic Sr_2 absorption around 700 nm. These weaker features are thereby attributed to an atomic transition. Inspection of Fig. 1 shows that the $^1D_2$ state of Sr lies energetically close to the $^1P_1$ state. Indeed, overlaying this energy value[23] (20 149.685 cm^{-1}) as a dashed vertical line on the matrix absorption spectra allows for a confident assignment to be made. Thus, the strongest absorption features centred at 484.1, 492.2, and 505.4 nm in Ar, Kr, and Xe, respectively,

TABLE II. The photophysical characteristics of the emission of strontium dimer extracted for the data shown in Fig. 7 in the vicinity of the atomic $^3P_1 - {}^1S_0$ resonance transition at 689.4491 nm. The symbols used have the same meanings as those in Table I.

Sr_2		Excitation			Emission				
RG	Band	λ (nm)	ν (cm^{-1})	δ (cm^{-1})	λ (nm)	ν (cm^{-1})	δ (cm^{-1})	SS (cm^{-1})	τ_{obs} (ns)
Ar	1	405.6	24 655						
	2	707.5	14 134	−370	779.9	12 822	−1682	1312	15.5
Kr	1	409.5	24 420						
	2	725.4	13 785	−719	784.6	12 745	−1759	1040	
Xe	1	417.5	23 952						
	2	739.8	13 517	−987	787	12 706	−1798	811	

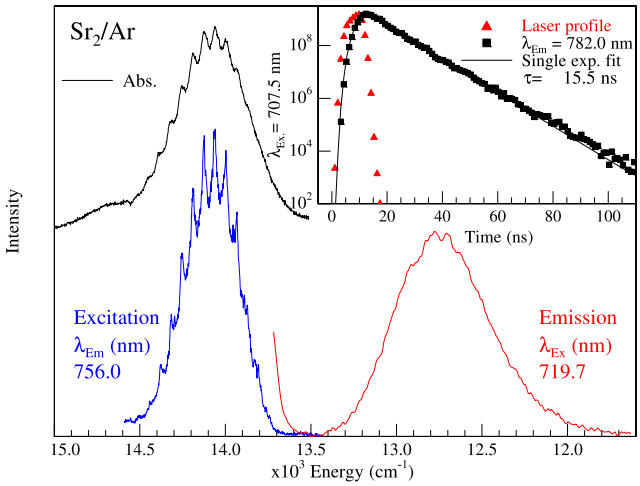

FIG. 8. A summary of the lowest energy strontium dimer emission recorded in solid argon with pulsed dye laser excitation. The black trace is the absorption spectrum while the blue trace is the laser induced fluorescence excitation spectrum recorded by monitoring the CCD emission at the specified wavelength. A kinetic slice of the time resolved emission spectrum is shown on a semi-log scale in the inset plot. The single exponential fit shown reveals an emission lifetime of 15.5 ns.

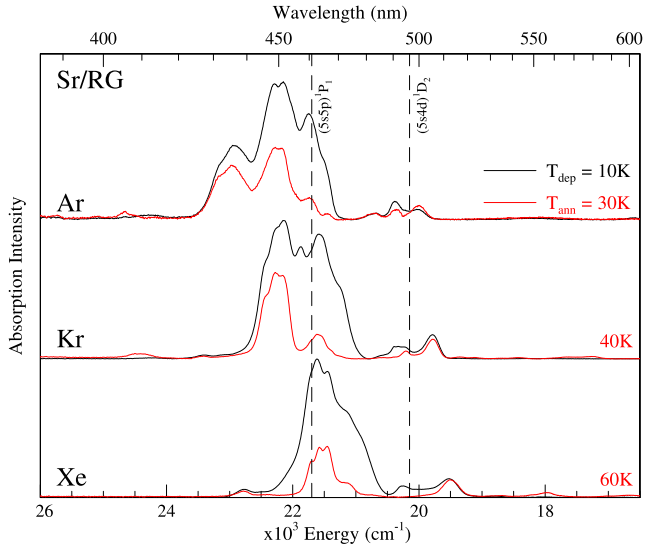

FIG. 9. A summary of the absorption spectra recorded at 10 K for the most dilute Sr/RG matrix systems in the visible spectral region. The black traces are the freshly deposited samples, while the red traces are those recorded after annealing to the specified temperatures in solid Ar, Kr, and Xe. The occurrence of the $^1D_2$ state absorption is evident in all three hosts in addition to the strong resonance $^1P_1$ state. Noteworthy is the removal of the red sites on the latter transition and the removal of the blue features on the $^1D_2$ state upon annealing.

are assigned to the parity-forbidden (5s4d) $^1D_2 \leftarrow (5s)^2\ ^1S_0$ transition of atomic Sr.

The results of annealing Sr/RG samples to the temperatures indicated in Fig. 9 are similar to those obtained in the Ba/RG systems in so far as red features are removed from the $^1P_1$ state transition. After annealing, a dominant threefold split band remains in Sr/Xe, a pair of structured bands are present in Sr/Kr, and at least three bands remain in Sr/Ar. The annealed Sr/Ar bands bear a strong resemblance to the equivalent transition in Ba/Ar (see the top trace in the right panel of Fig. 5). It is noteworthy that the $^1D_2$ state transitions exhibit the opposite annealing behaviour to the $^1P_1$ state in that the red features dominate on the former after annealing. This is especially evident in the case of Sr/Ar, but it is also true of the other RG systems shown in Fig. 9. Thus, after annealing, the matrix $^1D_2$ bands are all to the red of the gas phase transition while the $^1P_1$ bands are blue-shifted (with the exception of Xe). Since these two transitions share a common $^1S_0$ ground state, the differential shifting of the P and D states must indicate a net repulsive interaction on the $^1P_1$ and a slight attractive interaction on the $^1D_2$ state.

F. M-RG interaction potentials

The ground state PECs calculated for the Ba·RG, Sr·RG, and Ca·RG (RG = Ar, Kr, and Xe) diatomics at the CCSD(T) level of theory with the basis sets specified in Sec. II are presented in the three panels of Fig. 10. The computed equilibrium bond length (R_e) and dissociation energy (D_e) of the nine M·RG diatomics are collected in Table III and comparisons with existing data are provided in Table IV. Inspection of these values reveals long bond lengths in the range 5.15–5.62 Å for all the diatomics. For a given metal atom M, there is very little variation in the bond lengths for the three rare gases studied. For example, the equilibrium bond lengths for Ca·Ar, Ca·Kr, and Ca·Xe were determined to be 5.16, 5.15, and 5.17 Å, respectively. In the Sr·RG series, all the bond lengths are around 5.3 Å. The Ba·RG series presents a different situation where the 1:1 Xe complex presents the shortest bond length, 5.55 Å while the Ar complex is the longest at 5.62 Å. In contrast, the binding energies vary quite strongly between the rare gases—for Ca·RG values of 57, 86, and 130 cm^{-1} are found for RG = Ar, Kr, and Xe, respectively. For a given rare gas atom, the binding energies are fairly independent of the metal atom with M·Ar, M·Kr, and M·Xe values existing in the small range from 54.2 to 57.3, 84.0 to 86.5, and 129.7 to 132.3 cm^{-1}, respectively.

In contrast to the corresponding metal (M_2) and rare gas (RG_2) homonuclear diatomics, very little experimental data are available concerning the interaction potentials of the mixed M·RG diatomics. To the best of our knowledge, the only experimentally determined potentials come from the work of Breckenridge and co-workers.[25] In their study, laser excitation spectra were recorded for Ca·Ar, Sr·Ar, and Ba·Ar formed in a supersonic jet. Ground state well depths of 62 ± 10 and 68 ± 15 cm^{-1} were obtained from a Birge-Sponer extrapolation for Ca·Ar and Sr·Ar, respectively. Unfortunately, a similar analysis for Ba·Ar was not possible because the excitation spectrum of this complex was of poorer quality. The experimental binding energy obtained for Ca·Ar is in very good agreement with the current CCSD(T) result. While the agreement for Sr·Ar is less favourable, our *ab initio* dissociation energy lies within the quoted experimental error.

Theoretical investigations of the nine M·RG diatomics are also quite limited but what exists is collected in Table IV. The Ca·Ar 1:1 complex is the most studied of these systems and has been treated at varying levels of theory, ranging from *ab initio* methods such as CCSD(T),[26] Møller–Plesset (MP2),[27] configuration interaction (CI),[28] and multi-configurational

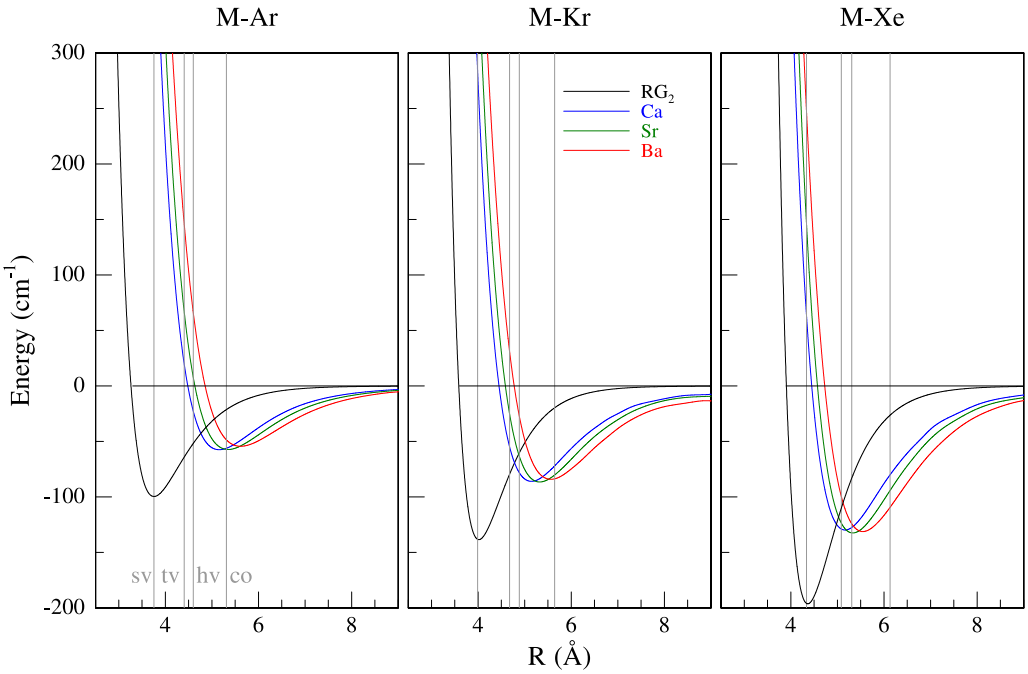

FIG. 10. A comparison of the three rare gas (RG_2) dimer potentials (black curves) with those calculated with the coupled-cluster method for the nine M·RG diatomics (coloured curves). The RG_2 potentials were generated with Morse functions using the parameters $D_e = 99.545$, 138.4, and 196.24 (cm^{-1}), $R_e = 3.7565$, 4.017, and 4.3634 (Å), and $\beta_e = 1.402\,18$, 1.604, and 1.509 ($Å^{-1}$) for Ar_2, Kr_2, and Xe_2, respectively. The large mismatch in the M·RG and RG_2 potentials is immediately evident in all three rare gases systems but especially so in Ar. The grey vertical lines show the sizes of the cubic sites in the solid rare gases considered to accommodate a spherical guest atom. The energies of the M·RG interactions at these sites are provided in Table III. It is only in the case of Ca-Xe that a possibility exists for single vacancy (SV) site occupancy, which has a very slight (64 cm^{-1}) repulsive interaction. For all the other M/RG systems, multi-vacancy (TV, HV, and CO) sites would be expected to occur.

self-consistent-field (MCSCF)[29] to an empirical method such as the Tang-Toennies (TT)[30] model potential. However, only two of these studies[26,30] extend to Ca·Kr and Ca·Xe. The most relevant comparison that can be made is with the work of Czuchaj *et al.*,[26] who computed the ground state Ca·RG PECs using a combined pseudopotential/CCSD(T) approach. R_e (Å)/D_e (cm^{-1}) values of 5.09/61.9, 5.05/97.5, and 5.17/131.4 were obtained for Ca·Ar, Ca·Kr, and Ca·Xe, respectively, which are in good agreement with the present determinations. More recently, Tang *et al.*[30] used the Tang-Toennies formula and combining rules to generate model potentials for the ground state Ca·RG diatomics, to obtain R_e (Å)/D_e (cm^{-1}) values of 5.10/72.7, 5.11/102.7, and 5.15/152.7 for RG = Ar, Kr, and Xe, respectively. Although the TT equilibrium bond lengths are in reasonable agreement with the present CCSD(T) values, the corresponding well depths are all more deeply bound.

Much less theoretical effort has been directed at the heavier M·RG complexes (M = Sr and Ba). The most extensive study of the Sr·RG diatomics was conducted by Tang

TABLE III. A summary of the molecular parameters of the M·RG diatomics (M = Ca, Sr, and Ba; RG = Ar, Kr, and Xe) extracted from the ground state interaction potentials, shown in Fig. 10 generated with coupled-cluster calculations. The columns on the right hand side provide the M-RG energies at the distances that exist by placing the metal atom in single vacancy (SV), tetravacancy (TV), hexavacancy (HV), and cubo-octahedral (CO) substitutional sites of the solid rare gas lattices. These distances are represented in Fig. 10 by the vertical grey lines for the *fcc* Ar, Kr, and Xe lattices.

		Diatomic		Energies of matrix sites (cm^{-1})			
M	RG	R_e (Å)	D_e (cm^{-1})	SV	TV	HV	CO
Ca	Ar	5.16	57.3	454.9	20.0	−22.3	−56.1
	Kr	5.15	85.9	282.6	−54.5	−78.0	−72.0
	Xe	5.17	129.7	64.3	−128.8	−127.4	−79.8
Sr	Ar	5.35	57.2	583.3	67.3	8.3	−57.1
	Kr	5.32	86.5	392.2	−24.7	−63.1	−80.1
	Xe	5.33	132.3	147.3	−123.4	−132.3	−94.1
Ba	Ar	5.62	54.2	695	146.5	66.8	−48.5
	Kr	5.57	84.0	504	31.7	−26.9	−83.7
	Xe	5.55	131.1	248.6	−99.3	−124.1	−109.3

TABLE IV. A comparison of the present CCSD(T) M·RG spectroscopic constants (highlighted in bold font) with existing theoretical and experimental data. The equilibrium bond lengths, R_e, are quoted in units of Angstrom (Å) and the dissociation energies, D_e, are given in wavenumbers (cm^{-1}).

System	R_e (Å)	D_e (cm^{-1})
Ca-Ar	**5.16**	**57.3**
	5.09[a]	61.9[a]
	4.995[b]	81.1[b]
	5.10[c]	72.7[c]
		62 ±10[e]
	4.86[f]	$D_0 = 87$[f]
	5.9[j]	72.6[g]
Kr	**5.15**	**85.9**
	5.05[a]	97.5[a]
	5.11[c]	102.7[c]
Xe	**5.17**	**129.7**
	5.17[a]	131.4[a]
	5.15[c]	152.2[c]
Sr-Ar	**5.35**	**57.2**
		68 ±15[h]
	5.38[d]	59.6[d]
	6.2[g]	63.5[g]
Kr	**5.32**	**86.5**
	5.38[d]	88.1[d]
Xe	**5.33**	**132.3**
Ba-Ar	**5.62**	**54.2**
	5.56[h]	73[h]
	5.36[i]	72.7[i]
Kr	**5.57**	**84.0**
	5.72[h]	80[h]
Xe	**5.55**	**131.1**
	5.93[h]	101[h]
	5.11[j]	427[j]

[a]Reference 26.
[b]Reference 27.
[c]Reference 30.
[d]Reference 31.
[e]Reference 25.
[f]Reference 28.
[g]Reference 29.
[h]Reference 32.
[i]Reference 33.
[j]Reference 34.

and co-workers,[31] where the metal — rare gas ground state interaction — was modelled using the TT empirical potential. The spectroscopic R_e (Å)/D_e (cm^{-1}) constants obtained from this approach were 5.38/59.6, 5.38/88.1, and 5.4/133.8 for Sr·Ar, Sr·Kr, and Sr·Xe, respectively. These values are in excellent agreement with the results of our present CCSD(T) calculations. As far as we are aware, only the Sr·Ar molecule has been studied using an *ab initio* method. A MCSCF calculation was carried out by Zhu *et al.*[29] for this system yielding a comparable ground state dissociation energy of 63.5 cm^{-1}, but a much longer equilibrium bond length of 6.2 Å.

The Ba·RG 1:1 complexes have been investigated by Czuchaj and co-workers,[32] who used CI/pseudopotential calculations to predict ground state R_e (Å)/D_e (cm^{-1}) values of 5.56/73.0, 5.72/80, and 5.93/101 for Ba·Ar, Ba·Kr, and Ba·Xe, respectively. In this case, the equilibrium bond lengths are systematically longer than the current coupled-cluster values and, aside from Ba·Ar, these potentials are more weakly bound. More recent computations have been conducted for Ba·Ar[33] and Ba·Xe[34] using a similar theoretical approach. While the ground state spectroscopic constants obtained for Ba·Ar (R_e = 5.36 Å and D_e = 72.7 cm^{-1}) are quite close to the original work of Czuchaj and co-workers,[32] the newer Ba·Xe ground state potential seems too deeply bound (R_e = 5.11 Å and D_e = 427 cm^{-1}).

IV. DISCUSSION

A. Metal dimer

The composition of matrix-isolated barium and strontium samples can, as presented in Figs. 3 and 6 for Ba/Ar and Sr/Ar, respectively, vary considerably depending on the deposition conditions used. Samples can be prepared composed almost exclusively of well-isolated atoms, showing little evidence of absorption bands attributable to higher aggregates. To this end, the deposition parameters such as window temperature and metal flux were systematically tuned to enhance especially dimer formation. As shown in Fig. 4, Ba/Xe is the most complicated of the three systems, presenting weak "satellite" features identifiable at 517.7, 525.6, and 606.1 nm, even under conditions which lead to very atomic Ar and Kr deposits. As these features lie spectrally close to dominant (6s6p) $^1P_1 \leftarrow {}^1S_0$ ($6s^2$) line, further investigation is provided with emission results shown in Fig. 4.

The resolved structure evident in Fig. 6 on the allowed $^1\Sigma_u \leftarrow {}^1\Sigma_g$ absorption transition of Sr_2, with a band maximum at 710 nm in Ar, was found to have an average spacing of approximately 64 cm^{-1}. This value represents the vibrational spacing in the first excited state of the dimer and matches earlier absorption results of Miller *et al.*[9,35] No resolved features are evident on the equivalent band of Ba_2. The spacing would be expected to be smaller in this case due to the increased mass of Ba compared with Sr. However, Lebeault *et al.*[22] extracted an excited state vibrational frequency (ω_e') of 65.2 cm^{-1} for Ba_2 in their R2PI data, quite similar to the Sr_2 value. A similar but slightly lower value of 59 cm^{-1} was predicted from Allouche's calculation.[36] The absence of structure in the metal dimer emission bands is consistent with the low fundamental (ω_e'') frequency of 33.2 cm^{-1} identified for Ba_2 from hot bands in the R2PI work.[22]

The emission behaviour observed for Ba dimer and Sr dimer is quite different as a comparison of Figs. 4 and 7 reveals. Thus, the emission of Sr_2 is in the vicinity of the lowest energy absorption at approximately 750 nm exhibiting resolved vibrational structure in excitation and Stokes shifts that are only weakly dependent on the matrix host. In contrast, Ba_2 does not produce any emission with resonance excitation into its lowest observed absorption band (band I in Fig. 3). This would suggest non-radiative transitions are competing very efficiently with fluorescence. Thus, the absence of resolved vibrational structure for Ba_2 may indicate lifetime broadening consistent with the absence of observed fluorescence in the matrix work. A possible reason for this behaviour is the higher

density of molecular states which exist for barium dimer in this region due to the large number of atomic asymptotes in the vicinity of the ^{3}P levels. As the comparison of the atomic energy levels shown in Fig. 1 reveals, Ba is much more congested in this spectral region than either Ca or Sr.

B. Metal atoms

The absorption spectra recorded for Sr and Ba are compared in Fig. 11 on the basis of three materials Ar, Kr, and Xe used as host solids. For the purposes of comparison, the absorption spectra of Ca have also been included in that figure. All the spectra have been centered on the relevant atomic $np\ ^1P_1 \leftarrow ns\ ^1S_0$ resonance transitions where n = 4, 5, and 6 for Ca, Sr, and Ba, respectively. Atomic Ca and Sr also exhibit $^1D_2 \leftarrow {}^1S_0$ absorption in the spectral regions shown and the locations of these gas phase transitions are indicated by the labels provided. All the spectra shown in Fig. 11 were recorded for annealed samples.

It is evident in Fig. 11 that in a given host, similar band structures exist for the three metal atoms. For instance, Ba/Ar exhibits three well defined bands all to the blue of the atomic transition. Sr/Ar has the same number of bands but with a gain in the intensity of the feature furthest to the blue. The enhancement of the furthest-blue band is most extreme in Ca/Ar where it dominates and the red band is now only a wing, located slightly to the red of the atomic $^1P_1 \leftarrow {}^1S_0$ transition. This behaviour points to similar sites occupied by the three metal atoms in Ar but populated in varying amounts leading to different intensity distributions.

A feature revealed in the comparisons shown in Fig. 11 is that the Ba/RG absorptions are consistently narrower than their Sr/RG and Ca/RG counterparts. This is especially evident in the M/Ar systems shown in the panel on the left. Based on the very similar van der Waals interactions (R_e and D_e values) identified in the CC calculations between the three metals and a given rare gas (see left panel in Fig. 10 for M-Ar potentials), this behaviour is simply related to the greater mass of atomic barium compared with the two other alkaline earth atoms. As a result, the effective phonon frequency coupling in the Ba/RG systems has a lower value than the other two metal atom systems. This in turn produces narrower absorption bands arising from the electron-phonon coupling which determines the line shapes of the transitions in the solid state spectra. In the M/Kr systems, a single feature dominates in Ca while a pair of well resolved bands exist in Sr. The Ca/Kr system exhibits a clear mirror image for the intensity patterns on the $^1P_1$ and the $^1D_2$ states. Based on the behaviour observed on the Sr/Kr system, Ba/Kr likely has two bands that are extensively overlapped. For the M/Xe spectra, single atomic features appear to dominate all three systems. The existence of weak dimer bands approximately 1000 cm^{-1} to the blue of the atomic resonance is a recurring feature in the absorption profiles of all the annealed xenon samples shown in Fig. 11.

The $^1D_2 \leftarrow {}^1S_0$ absorptions of Sr and Ca atoms shown in Fig. 11 also exhibit site structure but it is noteworthy that the intensity pattern is the reverse of that on the $np\ ^1P_1 \leftarrow ns\ ^1S_0$ resonance transitions just described. Thus, in Ca/Ar, the D band with the greatest intensity is furthest to the red, while it is the most-blue band on the P state. This reversal behaviour of the intensity patterns on the P and D states is best demonstrated in the Sr/Kr scan shown in the middle panel, where the red band dominates the D state while the blue, three-fold split feature dominates the P state absorption.

C. Site occupancy

A feature immediately evident in Fig. 10 is the pronounced mismatches which exist between the M·RG potentials (coloured traces) and those of the corresponding rare gas dimers (RG_2) shown by the black traces. Thus, the binding energies of the rare gas dimers are all greater than the heteronuclear diatomics but more significantly for site occupancy, the M·RG potentials all have their minima at

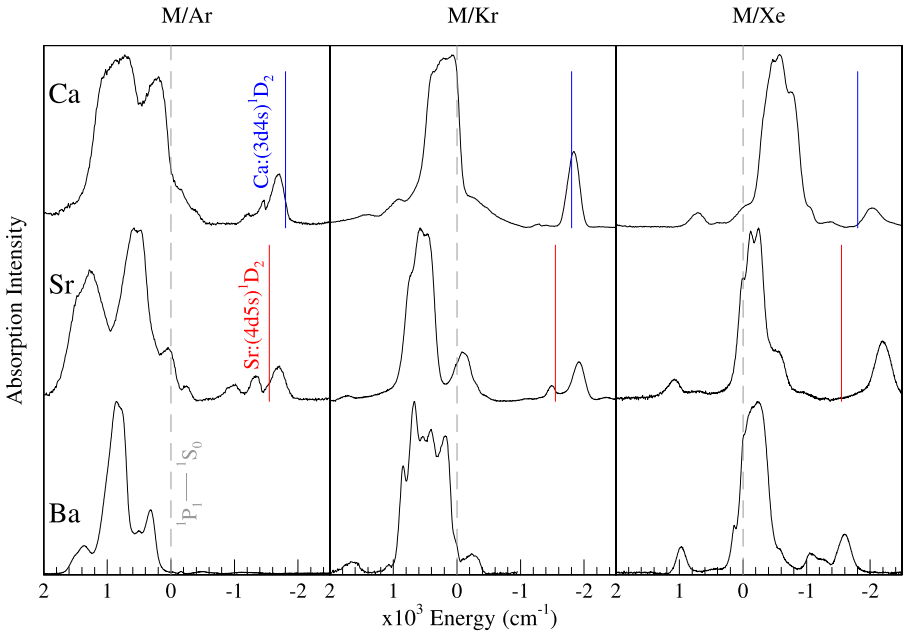

FIG. 11. A summary of the absorption spectra recorded at 10 K for the alkaline earth metal atoms Ca, Sr, and Ba in the annealed solid rare gases Ar, Kr, and Xe. To facilitate comparison, the spectra have been zeroed around the gas phase positions of the resonance $ns^1\ np^1\ ^1P_1 \leftarrow ns^2\ ^1S_0$ transitions (n = 4, 5, and 6 for Ca, Sr, and Ba) at 23 652.304, 21 698.452, and 18 060.261 cm^{-1}, respectively, and are all shown on the same energy scale. The positions of the $^1D_2$ level which also absorbs in this region for both Sr and Ca are shown for these two metal atoms.

nuclear separations greatly in excess of the rare gas dimers. This latter characteristic has profound implications on the possible sites occupied by the heavy alkaline earth metal atoms in the solid rare gases. The sizes of the "cubic" vacancies in the sRGs capable of accommodating the spherical ground state $^1S_0$ metal atoms are indicated by the vertical grey lines. The energetics determined from the calculated M·RG potentials for single vacancy (SV) and multi-vacancy (tetravacancy (TV), hexavacancy (HV), and cubo-octahedral (CO) substitutional) site occupancies are provided in Table III. From the numbers listed there, none of the M/RG matrix systems would be expected to have SV occupancy with the possible exception of Ca/Xe which only has a very slight (64 cm^{-1}) repulsive interaction. For all the other M/RG systems TV site occupancy would be predicted with the exception of Ba/Ar. In this system, attractive M-Ar interactions are only experienced in the large CO substitutional site which involves the removal of a central Ar atom and 12 of its nearest neighbours. However, even in this system, smaller sites such as HV may be occupied because of the requirement for lattice stabilisation. This arises because the removal of a large numbers of atoms to generate the bigger HV and CO sites (6 and 13 atoms, respectively) destabilises the host due to the loss of lattice atom-atom interactions. MD simulations have shown that "cramped" guest occupancy occurs much more favourably than occupancy in spacious sites. The driving force is maintenance of the overall lattice energy and a good compromise (which allows for some reduction in guest-host repulsion) is occupancy in cramped sites. A more detailed analysis of site occupancy is currently being undertaken with molecular dynamics calculations.

V. CONCLUSIONS

In contrast to our recent Eu/RG work,[37] which demonstrated the production of matrix-isolated Eu cations after laser irradiation, the Ba/RG matrices prepared in this work do not contain any Ba ions in the samples prepared either by thermal vaporisation or e-bombardment. Several of the bands attributed to "candidate" Ba ions in the recent Ba/Ar and Ba/Xe matrix work published in Ref. 8 appear to arise from Sr contamination in the barium metal. Fortuitously, the existence of strontium as an impurity in barium metal has proven to be an asset since it has allowed a detailed comparison to be made between the absorption spectra of these two, closely related but complex matrix systems. The complexity relates to the multi-site nature of the isolation of these large metal atoms in the solid rare gases as well as the luminescence characteristics of metal dimers of Sr and Ba.

Annealing of freshly deposited M/RG matrix samples has a pronounced effect on the absorption spectra in that the red features present on the $np\ ^1P_1 \leftarrow ns\ ^1S_0$ resonance transitions are removed. In contrast, the blue features are removed on the $nd\ ^1D_2 \leftarrow ns\ ^1S_0$ transitions in Sr and Ca. The red features on the $^1P_1$ transition are attributed to large multi-vacancy sites in the host solid. Thus, the contrasting behaviour points to a net repulsive guest-host interaction in the $^1P_1$ level and a net attractive interaction in the $^1D_2$ level. The bands structure remaining in a given host solid after annealing bears a strong resemblance amongst the three metals studied with the bands differing only in intensity. This points to the same sites being occupied by the metal atoms but in different amounts.

Ground state interaction potentials calculated with coupled-cluster methods for the nine M·RG diatomics have revealed bond lengths considerably greater than those of the rare gas dimers. A consequence of these mismatches is that the isolation of the heavier alkaline earth metal atoms in single substitutional sites of the solid rare gases is unlikely, with the possible exception of Ca in Xe. The cc results reveal that Ba·Xe complex has the shortest bond length of the three rare gases (Ar, Kr, and Xe) calculated—an exceptional result.

The luminescence of the metal dimer absorption bands of barium and strontium has been recorded revealing very different behaviours. Resonance fluorescence, with a lifetime of 15 ns, is observed for the lowest energy transition of Sr_2 while this transition is completely quenched in Ba_2. This behaviour is consistent with the absence of vibrational structure on the Ba_2 absorption band—indicating lifetime broadening arising from efficient relaxation to lower lying molecular states of the dimer. The density of molecular states in this spectral region is much greater for Ba_2 than for Sr_2 due to the large number of atomic ^1D and ^3D asymptotes which exist for the former and are absent in the latter.

ACKNOWLEDGMENTS

This research was partly funded by the John and Pat Hume award at N.U.I.-Maynooth which supported the Ph.D. studentship of Barry Davis. Dr. Martin Collier's help for recording the calcium matrix spectra shown in Fig. 11 is kindly acknowledged. We are grateful also to Professor Tim Wright and Dr. Adrian Gardner for sharing unpublished results of their calculations on the Ba·RG diatomics.

[1]E. Loginov and M. Drabbels, J. Chem. Phys. **136**, 154302 (2012).
[2]X. Zhang and M. Drabbels, J. Chem. Phys. **137**, 051102 (2012).
[3]V. Lebedev, P. Moroshkin, and A. Weis, Phys. Rev. A **84**, 022502 (2011).
[4]J. Visticot *et al.*, J. Chem. Phys. **100**, 158 (1994).
[5]M. Briant, M. A. Gaveau, and J. M. Mestdagh, J. Chem. Phys. **133**, 034306 (2010).
[6]A. Masson, L. Poisson, M. A. Gaveau, B. Soep, J. M. Mestdagh, V. Mazet, and F. Spiegelman, J. Chem. Phys. **133**, 054307 (2010).
[7]L. Balling and J. Wright, J. Chem. Phys. **83**, 2614 (1985).
[8]nEXO Collaboration, Phys. Rev. A **91**, 022505 (2015).
[9]J. C. Miller, R. L. Mowery, E. R. Krausz, S. M. Jacobs, H. W. Kim, P. N. Schatz, and L. Andrews, J. Chem. Phys. **74**, 6349 (1981).
[10]B. Healy, P. Kerins, and J. G. McCaffrey, Low Temp. Phys. **38**, 679 (2012).
[11]M. A. Collier and J. G. McCaffrey, J. Chem. Phys. **122**, 184507 (2005).
[12]M. A. Collier and J. G. McCaffrey, J. Chem. Phys. **119**, 11878 (2003).
[13]M. Valiev *et al.*, Comput. Phys. Commun. **181**, 1477 (2010).
[14]K. A. Peterson, D. Figgen, E. Goll, H. Stoll, and M. Dolg, J. Chem. Phys. **119**, 11113 (2003).
[15]EMSL Basis Set Exchange (v1.2.2) available at: https://bse.pnl.gov/bse/portal.
[16]H. Li *et al.*, Mol. Phys. **111**, 2292 (2013).
[17]Correlation Consistent Basis Sets for Ca, Sr, Ba, and Ra, available at: http://tyr0.chem.wsu.edu/~kipeters/basissets/alkali-pp.html.
[18]I. S. Lim, H. Stoll, and P. Schwerdtfeger, J. Chem. Phys. **124**, 034107 (2006).
[19]S. F. Boys and F. Bernardi, Mol. Phys. **100**, 65 (2002).
[20]S. l. Simon, M. Duran, and J. J. Dannenberg, J. Chem. Phys. **105**, 11024 (1996).
[21]R. Kresse, U. Baudis, P. Jäger, H. H. Riechers, H. Wagner, J. Winkler, and H. U. Wolf, *Ullmann's Encyclopedia of Industrial Chemistry* (Wiley-VCH Verlag GmbH & Co. KGaA, 2000).

[22]M. A. Lebeault, J. Viallon, V. V. Boutou, and J. Chevaleyre, J. Mol. Spectrosc. **192**, 179 (1998).
[23]A. Kramida, Y. Ralchenko, J. Reader, and NIST ASD Team, NIST Atomic Spectra Database (ver. 5.2), National Institute of Standards and Technology, Gaithersburg, MD, 2015, available at: http://physics.nist.gov/asd.
[24]B. Davis and J. G. McCaffrey, "Sr atom emission in the solid rare gases" (unpublished).
[25]A. Kowalski, D. J. Funk, and W. H. Breckenridge, Chem. Phys. Lett. **132**, 263 (1986).
[26]E. Czuchaj, M. Krośnicki, and H. Stoll, Chem. Phys. **292**, 101 (2003).
[27]K. N. Kirschner, J. Chem. Phys. **112**, 10228 (2000).
[28]F. Spiegelman, L. Maron, W. H. Breckenridge, J.-M. Mestdagh, and J.-P. Visticot, J. Chem. Phys. **117**, 7534 (2002).
[29]R.-S. Zhu, K.-L. Han, J.-H. Huang, J.-P. Zhan, and G.-Z. He, Bull. Chem. Soc. Jpn. **71**, 2051 (1998).
[30]D. D. Yang, P. Li, and K. T. Tang, J. Chem. Phys. **131**, 154301 (2009).
[31]G. P. Yin, P. Li, and K. T. Tang, J. Chem. Phys. **132**, 074303 (2010).
[32]E. Czuchaj, F. Rebentrost, H. Stoll, and H. Preuss, Theor. Chem. Acc. **100**, 117 (1998).
[33]K. Issa, R. Dardouri, and B. Oujia, J. Surf. Interfaces Mater. **1**, 15 (2013).
[34]K. Abdessalem, L. Mejrissi, N. Issaoui, B. Oujia, and F. X. Gadea, J. Phys. Chem. A **117**, 8925 (2013).
[35]J. C. Miller and L. Andrews, J. Chem. Phys. **69**, 936 (1978).
[36]A. R. Allouche, M. Aubert-Frécon, G. Nicolas, and F. Spiegelmann, Chem. Phys. **200**, 63 (1995).
[37]O. Byrne, B. Davis, and J. G. McCaffrey, J. Chem. Phys. **142**, 054307 (2015).